Platonic and Archimedean geometries in multicomponent elastic membranes

Graziano Vernizzi[a,1], Rastko Sknepnek[a], and Monica Olvera de la Cruz[a,b,c,2]

[a]Department of Materials Science and Engineering, Northwestern University, Evanston, IL 60208; [b]Department of Chemical and Biological Engineering, Northwestern University, Evanston, IL 60208; and [c]Department of Chemistry, Northwestern University, Evanston, IL 60208

Edited by L. Mahadevan, Harvard University, Cambridge, MA, and accepted by the Editorial Board February 8, 2011 (received for review August 30, 2010)

Large crystalline molecular shells, such as some viruses and fullerenes, buckle spontaneously into icosahedra. Meanwhile multicomponent microscopic shells buckle into various polyhedra, as observed in many organelles. Although elastic theory explains one-component icosahedral faceting, the possibility of buckling into other polyhedra has not been explored. We show here that irregular and regular polyhedra, including some Archimedean and Platonic polyhedra, arise spontaneously in elastic shells formed by more than one component. By formulating a generalized elastic model for inhomogeneous shells, we demonstrate that coassembled shells with two elastic components buckle into polyhedra such as dodecahedra, octahedra, tetrahedra, and hosohedra shells via a mechanism that explains many observations, predicts a new family of polyhedral shells, and provides the principles for designing microcontainers with specific shapes and symmetries for numerous applications in materials and life sciences.

crystalline shells | self-assembly

Uniform convex polyhedra, such as Platonic and Archimedean solids, have beguiled scientists, philosophers, and artists for millennia (1, 2). In our modern era, they are incorporated in the revolutionary Descartes's geometrization of nature and introduce aesthetic elements in the physical sciences (3). Although mathematicians have rigorously captured the "morphological essence" of such highly regular polytopes by classifying and formalizing their symmetries and isometries (4), the search for such structures in the realm of nature has been, for the most part, rather elusive.

Notable attempts include Plato's description of the fundamental matter constituents (5) and Kepler's effort to fit the motion of planets by using those very same regular solids that Greeks identified centuries earlier (6). In recent times, polyhedral shapes have been identified at the microscopic level. Besides faceted small metal clusters (7) and hard-sphere clusters (8), there are many examples of polyhedral shells ranging from capsids of viruses (9), supramolecular organic and inorganic assemblies (10), "platonic" hydrocarbons and carbon molecules (11, 12), to protein-based bacterial organelles (13) including carboxysomes (14, 15) and multicomponent ligand assemblies (16), to name a few. The connection between the lowest-energy configuration of a complex system at the microscopic scale and geometric principles has fostered many scientific discoveries (17), and it is a guiding principle in advancing modern fundamental science (18). We explore this connection here to design a previously undescribed family of polyhedral shells.

The most frequently observed polyhedral symmetry in self-assembled homogeneous elastic shells is the icosahedron, a polyhedron with the highest possible symmetry. A quantitative explanation of this account comes from the theory of elasticity (19, 20), which describes how any spherical shell made of a homogenous, isotropic, elastic material can *buckle* into an icosahedron. The onset of such faceting is controlled by a single parameter, the Föppl–von Kármán number $\gamma = YR^2/\kappa$ (19), where Y is Young's modulus, κ is the bending rigidity, and R is the radius of the shell. Closed membranes with the topology of a sphere cannot be covered by a perfect triangular crystalline lattice; that is, it is not possible to construct a lattice on the surface of a sphere such that each site has only six neighbors. Consequently, any such crystalline lattice will contain defects. If one allows for fivefold defects only then, according to the Euler theorem, the minimum number of defects is 12 fivefold disclinations. In the absence of further defects (21), these 12 disclinations are positioned on the vertices of an inscribed icosahedron (22). Because of the presence of disclinations, the ground state of the shell has a finite strain that grows with the shell size. When $\gamma > \gamma^*$ ($\gamma^* \sim 154$) any *flat* fivefold disclination buckles into a conical shape (19). On a spherical shell these 12 defects buckle simultaneously, and the spherical shell acquires an icosahedral shape (the only regular polyhedron with 12 vertices) (20).

Elastic theory assigns a curvature energy to regions of out-of-plane shell deformations (23). The faceting transition occurs when the curvature energy concentrates on special areas (edges and vertices) that are separated by flat domains (faces), instead of being uniformly distributed over the surface of a sphere. The condensation of the curvature energy is insightfully interpreted (24) as an example of *energy focusing* (25), and it is typical of the more general process of surface crumpling (26). As shown below, these concepts are crucial in the formation of heterogeneous polyhedral shells.

Most studies have pointed out the transition from sphere to icosahedron for a single-component elastic membrane and dismissed the possibility of a transition toward other types of uniform polyhedra. We find that it is possible to facet crystalline shells (including closed tethered membranes and spherical elastic meshworks) into shapes with symmetries other than icosahedral when we include elastic heterogeneities via increasing the number of the shell components with different elastic properties. Various proteins in cellular environments are coassembled into regular and irregular polyhedra shells, such as in energy-converting organelles and bacteria proteinaceous microcompartments (27). Moreover, heterogeneous membranes are also generated by coassembling cationic and anionic lipids into vesicles that are faceted regular and irregular polyhedra (28). In this work, we take the simplest case of a membrane composed of *two* components A and B that are individually isotropic and characterized by their Young's modulus, Y_A, Y_B, Poisson ratio ν_A, ν_B , and bending rigidity κ_A, κ_B. Such a case also describes multicomponent systems that segregate into two phases (29). Nevertheless, when multicomponent systems can access more than two phases, we expect more complex structures.

Author contributions: G.V. and M.O.d.l.C. designed research; G.V. developed the theoretical model; R.S. implemented the Monte Carlo simulations; G.V., R.S., and M.O.d.l.C. analyzed results; and G.V., R.S., and M.O.d.l.C. wrote the paper.

The authors declare no conflict of interest.

This article is a PNAS Direct Submission. L.M. is a guest editor invited by the Editorial Board.

Freely available online through the PNAS open access option.

[1]Present address: Department of Physics and Astronomy, Siena College, Loudonville, NY 12211.

[2]To whom correspondence should be addressed. E-mail: m-olvera@northwestern.edu.

This article contains supporting information online at www.pnas.org/lookup/suppl/doi:10.1073/pnas.1012872108/-/DCSupplemental.

A key feature of this model is that we do not assume the position of the components on the shell but only fix the relative fraction f of the two components to find the lowest-energy configuration. We associate with any distribution of the two components over the shell a standard elastic energy that depends also on the actual shape of the shell, which we parameterize by using a popular discretized model for elastic membranes based on a triangulated spherical mesh (30). In our discrete model, f is the fraction of B bonds over the total number of bonds (A- and B-type only) on the shell (in a continuum model f would be the area fraction). We therefore minimize the elastic energy by (*i*) letting the two components freely distribute over the surface at a fixed relative fraction f and (*ii*) allowing the overall shell shape to change and adapt in three dimensions accordingly. The lowest-energy configurations are obtained by means of a series of standard Monte Carlo simulated annealing simulations. Similar to other studies (19, 20), we consider only shells with a convex shape. The possibility of having more general geometries including blebs, buds, and saddle shapes require the presence of defects (30), which proliferate at high temperatures (31). For simplicity, we assume here that thermal fluctuations are negligible compared to the elastic and bending energies.

Results and Discussion

We reduce the parameter space (with tunable f, Y_A, Y_B, ν_A, ν_B, κ_A, and κ_B) by considering materials with the same and most common value of the Poisson ratio, $\nu_A = \nu_B \sim 0.33$. In order to demonstrate the family of possible buckled structures, we consider components A, B such that if the shell is covered completely by one of them, its stable shape would be either icosahedral or spherical. A sufficient condition for that to happen is to choose $\kappa_B > \kappa_A$ such that either $\gamma_B < \gamma^* < \gamma_A$ or $\gamma_A < \gamma^* < \gamma_B$, where $\gamma_A = Y_A R^2/\kappa_A$ and $\gamma_B = Y_B R^2/\kappa_B$. In what follows, we consider the B component to be more rigid than the A component ($\kappa_B > \kappa_A$).

At intermediate values of the fraction f, the tendency of one component to achieve a spherical shell competes with the preference of the other component for an icosahedral shape. We explore this region in detail in Fig. 1. From the snapshots, one can observe the existence of uncommon polyhedral structures at intermediate values of f. The existence of such structures is surprising, because the classic theory of buckling for a spherical shell identifies the 12 fivefold disclinations arranged in icosahedral symmetry, by assumption, as the seeds for the conical shapes that evolve into the vertices of an icosahedron during faceting. All polyhedra snapshots in Figs. 1 and 2 have 12 fivefold disclinations as required by Euler theorem, but they are arranged in different positions, and they do not act as seeds for buckling (meaning that they are not located on the polyhedra vertices). For example, in the tetrahedron, there are three disclinations per face positioned farthest away from one another and are actually slightly sunken into the faces, as can be seen in mean curvature maps in Fig. 3, where we also show how the curvature concentrates along the edges of the faceted structures. Therefore, an unconventional buckling mechanism is required to describe faceted multicomponent shells, such as the polyhedra observed in bacterial microcompartments (27), which are remarkably similar to the polyhedra snapshots we find, as shown in Fig. 1 (see also figure 4 in ref. 32 and figures 7 *a–d* in ref. 15).

When two elastic components are sharing a surface that includes fivefold disclinations, they tend to segregate. On a sphere, the B component with a higher bending rigidity is repelled equally by all 12 disclinations and, therefore, roughly tends to be confined in regions that are dual to the icosahedron, namely, the spherical dodecahedron. Such an argument is an approximation, because it depends on the values of the fraction f and the Y_A/Y_B ratio, set to one in Fig. 1 for simplicity. The region around the edges connecting the vertices, where one expects the curvature energy to be high, tends to be occupied by the component with a smaller bending rigidity (component A), whereas the flat regions corresponding to the polyhedral faces tend to be occupied by the component with a higher bending rigidity (component B).

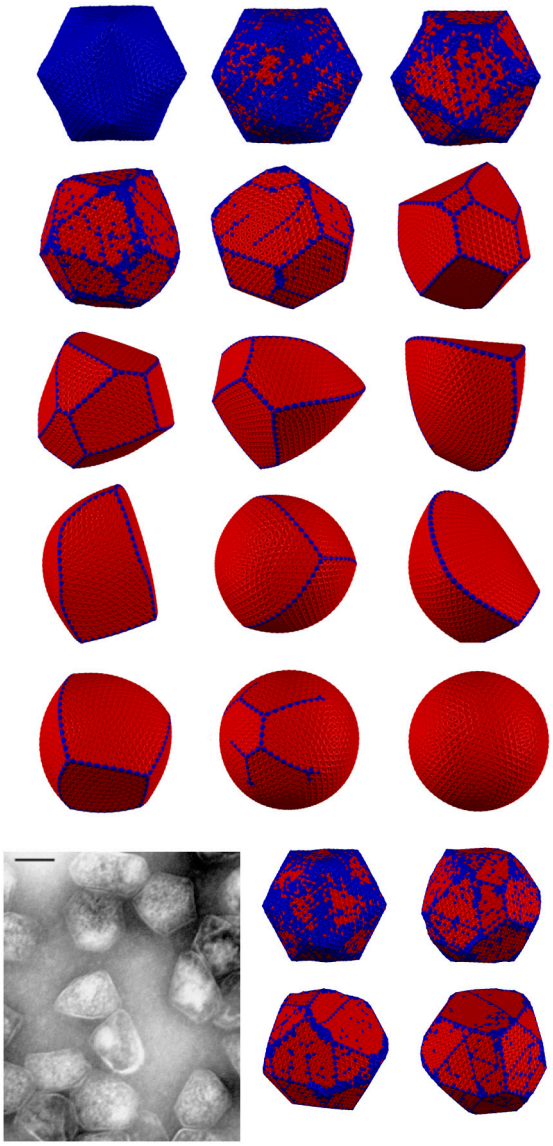

Fig. 1. Snapshots of configurations of coassembled shells at different fraction f where the A component (in blue) has $Y_A = 5.77$, and $\kappa_A = 0.06$, whereas the B component (in red) has $Y_B = 5.77$, and $\kappa_B = 28.9$, and the radius of the shell is about $R \sim 11.3$ in units of the average bond length. In the snapshots in the top five rows, the fraction f varies (*Left* to *Right*, and *Top* to *Bottom*) as $f = 0$,0.2, 0.5, 0.7, 0.85, 0.95, 0.955, 0.965, 0. 97, 0.975, 0.977, 0.98, 0.985, 0.99, and 1. The electron micrograph of purified Pdu microcompartments from *Salmonella enterica* (scale bar: 100 nm) [Reproduced with permission from ref. 27] (*Bottom Left*) shows cellular shells that resemble the coassembled polyhedra shells shown here. (*Bottom Right*) Four additional snapshots of inhomogeneous coassembled shells (for the same parameters as above) the fraction f increases (*Left* to *Right*, *Top* to *Bottom*) as $f = 0.3$, 0.65, 0.75, and 0.8.

At intermediate values of the relative fraction f, the interplay between geometrical shapes and patterns on the surface starts to burgeon. The component with low-bending rigidity tends to grow along arcs. This would be also the case of a component with a larger Young's modulus, because bending without stretching favors a curved region with zero Gaussian curvature, which is a surface that locally has a flat direction. Such lines can merge into vertices, while still conforming to the underlying hexagonal

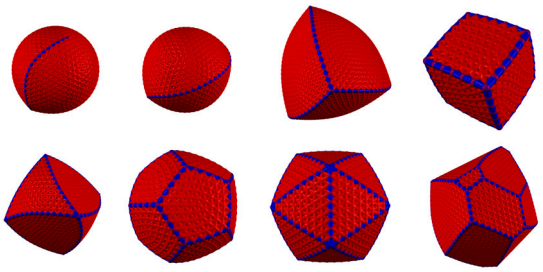

Fig. 2. Some examples of polyhedral structures we obtained by considering two different elastic components on a spherical shell. We note the exotic presence of the 1-hosohedron and 2-hosohedron (*Top Left*), and the truncated octahedron (slightly deformed, *Bottom Right*). The remaining structures are regular platonic solids: tetrahedron, cube, octahedron, dodecahedron, and icosahedron.

packing lattice. The resulting pattern of lines of one component around the sphere acts as the scaffold for the faceting of the shell into a polyhedral structure with regular threefold or fourfold vertices. Such vertices are joined together by sharp edges, occupied by component A, that surrounds polygons occupied by the high bending rigidity component B. These polygons tend to have a shape as uniform as possible. However, irregularities are unavoidable, because only very specific values of the fraction f fulfill the commensurability conditions that are necessary to obtain uniform and perfectly regular polyhedra. Interestingly, the segregation features in a flat disk with one fivefold disclination and with $Y_A < Y_B$ shows that, besides boundary effects, most of the stretching energy is condensed around the soft-component A at the fivefold disclination at the center of the disk (see *SI Appendix*). The segregation of the two elastic components around buckled conical disclinations, and over the ridges connecting them, is in general different from the planar case, most likely caused by the Gaussian curvature present in the spherical and absent in the planar case.

One can understand the qualitative origin of previously undescribed faceted geometries by recalling that any polyhedron with faces that are regular polygons and with congruent vertices must be a uniform polyhedron. The only convex uniform polyhedra are the 5 Platonic solids and the 13 Archimedean solids. At intermediate values of the fraction f, we find the tendency toward polyhedra that are less regular (with vertices with fewer degrees of symmetry called *Johnson* solids).

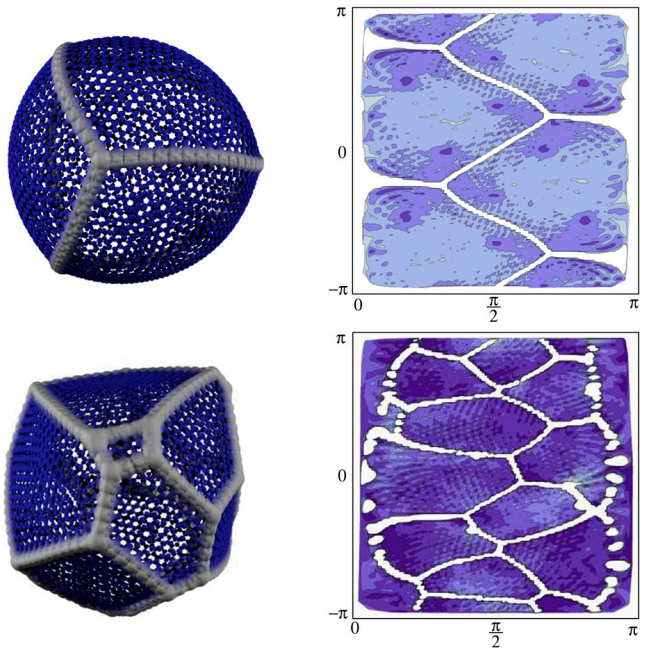

Fig. 3. The density plots of the mean curvature (*Right*, in spherical coordinates $0 \le \theta \le \pi$, $-\pi \le \varphi \le \pi$, with dark-color/low-density and bright-color/high-density) reveals how the curvature of the buckled shells (*Left*) *condenses* in correspondence to the softer elastic component.

Because the tendency of forming lines and edges is a consequence of the effective segregation between the two elastic components (even though the components are chemically compatible to be coassembled, they segregate due to their different elastic properties), such patterns occur also on a spherical shell that is rich in the component that does not favor buckling. In this case only spherical tilings arise, as polyhedral tessellations of the spherical surface. The most remarkable spherical tilings, which are observed in some instances at very low relative ratios, are the two-gonal and three-gonal hosohedra, which resemble cellular containers (15) and coassembled cationic and ionic amphiphiles with various degrees of ionization states per molecule (28). Such structures do not have a polyhedral counterpart with polygonal flat faces. Fig. 2 shows an extract of the portfolio of some structures we have found. The presence of a line tension term between the two components can change the scenario we describe in this paper and make it actually richer. For instance, at sufficiently high values of the line tension, single-component arcs would be suppressed in favor of larger domains, as shown in *SI Appendix*.

Concluding Remarks

In summary, once the homogeneity requirement is lifted, a unique buckling pathway for a two-component elastic shell is available. Depending on the relative fraction of the components, the shell minimizes its elastic energy with a number of regular shapes with symmetries other than icosahedral. A surprising feature of this model is that by slowly varying the relative fraction of the two elastic components, the lowest-energy configuration leaps from one polyhedral object to the next without following the path where the number of broken symmetries in the transition is minimal. A clear explanation of this fact is due to the strong constraints imposed in a finite size system. The various regular and irregular polyhedra we predict closely resemble the shapes observed in the multicomponent bacterial microcompartments such as Pdu (32). Moreover, polyhedra due to elastic inhomogeneities may also result upon adsorption of components or proteins to crystalline membranes or meshworks, such as cellular containers or clathrin cages (33), if they can considerably soften or harden the shell locally.

If the reported shapes are reproducible experimentally, then one can foresee intriguing potential technological applications that include the design of containers with shape recognition and/or with highly catalytic surfaces. The coassembled shells naturally develop surface patterns that lead to polyhedra shells with an enhanced concentration of the soft component at the polyhedra edges, rendering high functionality to the shells. Polyhedral heterogeneous elastic shells could pave the way toward a previously undescribed guiding principle for the control of shape at the nanometer and micron scale, and toward the rational design of functional nanocontainers to mimic, for example, protein-based *bacterial organelles* (13). A buckling approach to ionic icosahedral shells utilizing long-range electrostatic interactions was proposed earlier (34). However, the case we consider in this paper is based on simple local elastic interactions: As such, it represents also a previously undescribed paradigm for the faceting transition of spherical shells. Although large spherical and icosahedral shells are abundant in nature, the less symmetric polyhedral shells discovered here are potentially more functional and appear at the nanometer length scales where their functionality can be fully exploited, which suggests that evolution might have selected its cell components in an optimal way to take advantage of this previously unexplored buckling mechanism.

Model and Method

There is an extensive literature on discrete network models that can be used to effectively describe elastic membranes or thin shells (30). We adopted a standard discretization, which is based on a two-dimensional triangular lattice with equal-length bonds. The triangular lattice reproduces isotropic, homogeneous elastic properties in the continuum limit (i.e., when the number of triangles goes to infinity while the length of the discrete bonds goes to zero). The total stretching energy of the network is defined by a harmonic potential nearest-neighbor interaction:

$$F_s^{\text{discrete}} = \sum_{i\in\text{bonds}} \frac{\varepsilon_i}{2}(l_i - l_0)^2.$$

The stiffness constants ε_i are position-dependent variables and in our model can take only two values ε_A and ε_B, corresponding to the two components A and B, and they are associated to the *bonds* of length l_i of the triangulated surface. For simplicity, we set the nonstretched bond length to $l_0 = 1$. This choice differs from approaches used to study binary fluctuating membranes, where the components are placed either on the surface triangles (35) or on the vertices (36), because in our case both the stretching energy and the bending energy are bond-based quantities. The discrete bending energy is (19)

$$F_b^{\text{discrete}} = \sum_{i\in\text{bonds}} \frac{\kappa_i}{2}(\vec{n}_{i,1} - \vec{n}_{i,2})^2,$$

where $\vec{n}_{i,1}$ and $\vec{n}_{i,2}$ are the unit normal vectors of the two triangles that share the bond l_i.

The species A or B are naturally associated to the bond on which they are defined and because neither the number of bonds nor the connectivity of the membrane changes during the simulation, the total ratio of the A component over the B component remains constant without introducing any further constraint. The only additional energy contribution is a tether-and-bead potential that effectively ensures the self-avoidance of the membrane.

The relation between the discrete $F_s^{\text{discrete}}, F_b^{\text{discrete}}$ and the continuum energies F_s, F_b is not straightforward. In the limit of large number of triangles (19) F_b^{discrete} maps into F_b, with the identification $\kappa = \frac{\sqrt{3}}{2}\kappa_i$ for cylindrical, and $\kappa = \frac{1}{\sqrt{3}}\kappa_i$ for spherical shells (30). In general, such an identification is shape dependent (37). Moreover, the identification of the bond-based stretching energy F_s^{discrete} differs also slightly from the vertex-based counterpart derived earlier (19), which is $Y = 2\varepsilon/\sqrt{3}, \nu = 1/3$. In fact, under small deformations, the length of a bond l_i changes to $l_i' = \sqrt{(1 + 2u_{\alpha\beta})\delta x^\alpha \delta x^\beta} \approx l_0 + u_{\alpha\beta}\delta x^\alpha \delta x^\beta$ (23). By applying the Euler–Maclaurin formula $\sum_i f(x_i)\Delta \approx \int f(x)dx$ to the discrete stretching energy, we obtain

$$F_s^{\text{discrete}} = \sum_{i\in\text{links}} \frac{\varepsilon_i}{2}(l_i - l_0)^2 \approx \frac{1}{\Delta}\int d^2z \frac{\varepsilon(z)}{2}(u_{\alpha\beta}\delta x^\alpha \delta x^\beta)^2,$$

where the discrete element area is $\Delta = 2\frac{1}{3}\frac{\sqrt{3}}{4}l_0^2 = \frac{l_0^2}{2\sqrt{3}}$. We expect that, within a region occupied by a single component, the relation obtained in ref. 30 for homogeneous systems is still valid, and deviations might be relevant at the boundary between the two components. Therefore, in this work we assume $Y(z) = 2\varepsilon(z)/\sqrt{3}, \kappa(z) = \kappa_i/\sqrt{3}, \nu = 1/3$ for spherical shells, and $Y(z) = 2\varepsilon(z)/\sqrt{3}, \kappa(z) = \sqrt{3}\kappa_i/2, \nu = 1/3$ for cylindrical geometries and disks.

All calculations were performed using a Monte Carlo code that we developed. A typical shell contained up to $N_v = 2{,}000$ vertices, $N_e = 6{,}000$ edges, and $N_t = 4{,}000$ triangles. Starting from a spherical configuration with a random distribution of soft and hard components, the structure was relaxed by performing simulated annealing with a linear cooling schedule. To ensure that we find fully relaxed structures, we have performed up to 10 cooling cycles. A typical run contained 1 million Monte Carlo sweeps. Each sweep had two parts: (*i*) A move of each vertex was attempted, for a total of N_v random vertex moves, followed by (*ii*) N_v attempted edge swaps. In the second part, two edges were chosen at random and a swap of their types was attempted. A total of N_v such moves were made. We note that although there are more edges than vertices, i.e., $N_e > N_v$, for simplicity we opted to use the same number (N_v) of attempted Monte Carlo moves for both vertex moves and edge swaps. Vertex moves and edge swaps were accepted or rejected according to the Metropolis rules. Each run took close to 40 h on a single Intel Xeon E5520 processor at 2.4 GHz.

The buckling of a disk with two elastic components is particularly enlightening. When a membrane containing a disclination is allowed to deform away from the planar configuration, the stretching energy can convert into bending energy, with the consequent *buckling* of the membrane at the disclination (19). The bending energy is described by the classic Helfrich energy functional: $F_b = \int dS(\kappa H^2/2 + \kappa_G K)$, where H is the mean curvature (i.e., the sum of the principal curvatures), K is the Gaussian curvature (the product of the principal curvatures), κ and κ_G are the bending rigidity and the Gaussian rigidity, respectively, and dS is the area element of the curved surface. Note that we have assumed zero spontaneous curvature, $H_0 = 0$. The estimate of the bending energy of a membrane containing a disclination is considerably more complicated than the evaluation of the stretching energy, and even in the fully homogeneous case it can be solved exactly only in the inextensional limit (i.e., $Y \to \infty$): $F_b = s\kappa \log(R/l_0)$, where the native bond length l_0 acts as a short-distance cutoff parameter (19), and $s = \pi/5$ for a fivefold disclination. We can estimate the bending energy in such an "unstretchable" limit for the two-component case. A fivefold disclination at the center of a disk of radius R can be obtained by cutting away a circular sector with central angle $2\pi/6$, and subsequently gluing together the two newly formed edges (20, 24). In the case we are considering here, such a cut-and-glue operation yields a cone, with slanted height R, a circular base of radius $r = 5R/6$, and height $h = \sqrt{11}R/6$. Assuming a fully radial symmetry, we take the two components A and B having bending rigidities κ_A and $\kappa_B > \kappa_A$, respectively, that occupy two circular regions with one surrounding the other. Let the two regions have slanted heights R_1 (inner region, occupied by A) and $R > R_1$ (outer region occupied by B). The area fraction is therefore $f = R_1^2/R^2$. The (local) mean curvature of such a cone at a height z from the apex is $H = h^2/(rz\sqrt{r^2 + h^2}) = 11/30\ z$, whereas the Gaussian curvature is $K = 0$ everywhere, because the principal curvature along the radial direction remains zero even after buckling. The bending energy reads

$$\begin{aligned} F_b &= \int_{r<R_1} dS\frac{\kappa_A}{2}H^2 + \int_{R_1<r<R} dS\frac{\kappa_B}{2}H^2 \\ &= \frac{11\pi}{30}\left[\kappa_A Log\left(\frac{R_1}{a}\right) + \kappa_B Log\left(\frac{R}{R_1}\right)\right]. \end{aligned}$$

The similar case where the inner component is B and the outer component is A at fixed area fraction f can be obtained by simply substituting $\kappa_A \leftrightarrow \kappa_B, f \to 1 - f$. It is straightforward to verify that the latter case always has higher energy, when $R > 1/\sqrt{f(1-f)}$, which is always true for large R. We conclude that the softer component (i.e., one with smaller bending rigidity) tends to occupy the region containing the disclination.

One should consider also the possibility of breaking the circular symmetry, with the two components distributing nonuni-

formly around the buckled cone. This case would correspond to solving all the Föppl–von Kármán (FvK) equations with cylindrical symmetry and by considering all Fourier angular components (38). It is natural to assume that, for large disks, the curvature will condensate in the regions occupied by the softer component (A), because the energetic penalty of having higher curvature there is small. We therefore consider only the case where the disclination buckles into a pyramid. In such a case the curvature is concentrated on the edges of the pyramid (see Fig. 4), and it is proportional to approximately $|\hat{n}_i - \hat{n}_{i+1}| = h \sin\frac{\pi}{n}\sqrt{8/\left(2h^2 + r^2 + r^2\cos\frac{2\pi}{n}\right)}$, where $\hat{n}_i$ is the normal vector to the ith side of the pyramid, n is the number of sides of the pyramid, h is the height, and r is the radius of the polygonal base (discussed below). Once again, the inextensional limit fixes the radius $r = R\sin x/\sin z$, with $x = 5\pi/3n$ and $z = \pi/n$, and the height $h = \sqrt{R^2 - r^2}$. This implies a curvature along the edge proportional to $|\hat{n}_i - \hat{n}_{i+1}| = 2\sqrt{\sin x^2 - \sin z^2}/\cos x$, and, therefore, the total bending energy is $2nR\kappa_A(\sin x^2 - \sin z^2)/\cos x^2 \propto R$, which is a linear function of R because it grows with the length of the edges where the curvature is condensed.

Monte Carlo simulations at a low temperature for $f \sim 0.07$, $Y_A = 1.15$, $\kappa_A = 0.87$, $Y_B = 115$, $\kappa_B = 26$, and $R = 10$ (units of bond length in our discrete model) are shown in Fig. 4. The component A has an FvK ratio below the buckling transition and therefore favors flat configurations. However, the component B has an FvK ratio above the buckling transition and favors the out-of-plane buckling of the disclination. When one of the components is present at a sufficiently large fraction, the conical buckling breaks its rotational invariance and develops into a pyramidal shape. The intermediate cases $0 < f < 0.1$ show a rich behavior (see Fig. 7 in *SI Appendix*). At small area fraction, the soft component condenses along edges that radiates out of the fivefold disclination. Interesting patterns seem to arise spontaneously at intermediate values of f without the need of introducing any additional competing interaction among the components, such as a line tension. It appears that the component that is softer and weaker tends to accumulate around the center of disk, on top of the disclination when the geometry is planar, and along lines radiating out of the disclination along which the edges of a pyramidal configuration form. Such a mechanism is at the core of the formation of the more complex faceted shapes observed in this work.

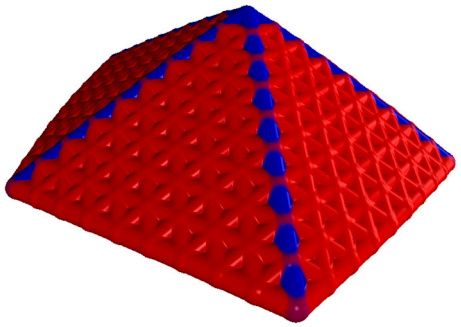

Fig. 4. Buckling of a fivefold disclination on a disk of radius $R = 10$ (units of bond length) into a pyramidal shape. The component in blue has elastic parameters, $Y_A = 1.15$, $\kappa_A = 0.87$, which favors flat configurations whereas the component in red has $Y_B = 115$, $\kappa_B = 26$, which favors buckled configurations. The relative fraction is $f = 0.07$. The figure is the result of 10^6 simulated annealing Monte Carlo sweeps.

ACKNOWLEDGMENTS. We thank Alfonso Mondragón for useful comments. G.V. and R.S. were supported by US Department of Energy Award DEFG02-08ER46539, and M.O.d.l.C. thanks the Air Force Office of Scientific Research for support by Award FA9550-10-1-0167.

1. Sutton D (2002) *Platonic & Archimedean Solids* (New York, Walker & Co) p 58.
2. Cromwell PR (1997) *Polyhedra* (Cambridge Univ Press, Cambridge, UK) p xiii.
3. McMorris N (1989) *The Natures of Science* (Associated Univ Presses, Rutherford, NJ).
4. Coxeter HSM (1973) *Regular Polytopes* (Dover Publications, New York), 3rd Ed, p xiii.
5. Plato Waterfield R, Gregory A (2008) *Timaeus and Critias* (Oxford Univ Press, Oxford, UK) p ixviii.
6. Kepler J, Aiton EJ, Duncan AM, Field JV (1997) *The Harmony of the World* (American Philosophical Society, Philadelphia, PA) p xli.
7. Marks LD (1994) Experimental studies of small-particle structures. *Rep Prog Phys* 57:603–649.
8. Meng GN, Arkus N, Brenner MP, Manoharan VN (2010) The free-energy landscape of clusters of attractive hard spheres. *Science* 327(5965):560–563.
9. Caspar DLD, Klug A (1962) Physical principles in construction of regular viruses. *Proceedings of the Cold Spring Harbor Symposia on Quantitative Biology*, 27 (Cold Spring Harbor Lab Press, Plainview, NY) p 1.
10. MacGillivray LR, Atwood JL (1999) Structural classification and general principles for the design of spherical molecular hosts. *Angew Chem Int Edit* 38:1019–1034.
11. Kroto HW, Heath JR, Obrien SC, Curl RF, Smalley RE (1985) C-60—Buckminsterfullerene. *Nature* 318:162–163.
12. Baughman RH, Galvao DS, Cui CX, Wang Y, Tomanek D (1993) Fullereneynes—A new family of porous fullerenes. *Chem Phys Lett* 204:8–14.
13. Tanaka S, Sawaya MR, Yeates TO (2010) Structure and mechanisms of a protein-based organelle in Escherichia coli. *Science* 327:81–84.
14. Yeates TO, Kerfeld CA, Heinhorst S, Cannon GC, Shively JM (2008) Protein-based organelles in bacteria: Carboxysomes and related microcompartments. *Nat Rev Microbiol* 6:681–691.
15. Iancu CV, et al. (2010) Organization, structure, and assembly of alpha-carboxysomes determined by electron cryotomography of intact cells. *J Mol Biol* 396:105–117.
16. Sun QF, et al. (2010) Self-assembled M24L48 polyhedra and their sharp structural switch upon subtle ligand variation. *Science* 328:1144–1147.
17. Muller A (2003) The beauty of symmetry. *Science* 300(5620):749–750.
18. Zee A (1999) *Fearful Symmetry: The Search for Beauty in Modern Physics* (Princeton Univ Press, Princeton, NJ) p xvi.
19. Seung HS, Nelson DR (1988) Defects in flexible membranes with crystalline order. *Phys Rev A* 38:1005–1018.
20. Lidmar J, Mirny L, Nelson DR (2003) Virus shapes and buckling transitions in spherical shells. *Phys Rev E* 68:051910.
21. Bowick MJ, Nelson DR, Travesset A (2000) Interacting topological defects on frozen topographies. *Phys Rev B* 62:8738–8751.
22. Zandi R, Reguera D, Bruinsma RF, Gelbart WM, Rudnick J (2004) Origin of icosahedral symmetry in viruses. *Proc Natl Acad Sci USA* 101:15556–15560.
23. Landau LD, Lifshits EM (1970) *Theory of Elasticity* (Pergamon Press, Oxford, NY), 2nd Ed, p viii.
24. Witten TA, Li H (1993) Asymptotic shape of a fullerene ball. *Europhys Lett* 23:51–55.
25. Witten TA (2007) Stress focusing in elastic sheets. *Rev Mod Phys* 79:643–675.
26. Lobkovsky A, Gentges S, Li H, Morse D, Witten TA (1995) Scaling properties of stretching ridges in a crumpled elastic sheet. *Science* 270:1482–1485.
27. Fan CG, et al. (2010) Short N-terminal sequences package proteins into bacterial microcompartments. *Proc Natl Acad Sci USA* 107:7509–7514.
28. Greenfield MA, Palmer LC, Vernizzi G, de la Cruz MO, Stupp SI (2009) Buckled membranes in mixed-valence ionic amphiphile vesicles. *J Am Chem Soc* 131:12030.
29. Huang C, Delacruz MO, Swift BW (1995) Phase-separation of ternary mixtures—Symmetrical polymer blends. *Macromolecules* 28:7996–8005.
30. Nelson DR, Piran T, Weinberg S (2004) *Statistical Mechanics of Membranes and Surfaces* (World Scientific, River Edge, NJ), 2nd Ed, p xvi.
31. Bowick M, Shin H, Travesset A (2004) Dynamics and instabilities of defects in two-dimensional crystals on curved backgrounds. *Phys Rev E* 75:8.
32. Cheng SQ, Liu Y, Crowley CS, Yeates TO, Bobik TA (2008) Bacterial microcompartments: their properties and paradoxes. *Bioessays* 30:1084–1095.
33. Dell'Angelica EC (2001) Clathrin-binding proteins: Got a motif? Join the network! *Trends Cell Biol* 11:315–318.
34. Vernizzi G, de la Cruz MO (2007) Faceting ionic shells into icosahedra via electrostatics. *Proc Natl Acad Sci USA* 104:18382–18386.
35. Kumar PBS, Gompper G, Lipowsky R (2001) Budding dynamics of multicomponent membranes. *Phys Rev Lett* 86:3911–3914.
36. Kumar PBS, Rao M (1998) Shape instabilities in the dynamics of a two-component fluid membrane. *Phys Rev Lett* 80:2489–2492.
37. Gompper G, Kroll DM (1996) Random surface discretizations and the renormalization of the bending rigidity. *J Phys I* 6:1305–1320.
38. Mitchell LH, Head AK (1961) The buckling of a dislocated plate. *J Mech Phys Solids* 9:131–139.